Surfaces and Interfaces 58 (2025) 105847

Contents lists available at ScienceDirect

Surfaces and Interfaces

journal homepage: www.sciencedirect.com/journal/surfaces-and-interfaces

Distinct mechanisms for the underwater adhesions of Pvfp-5β and Mfp-5: A comparative all-atom molecular dynamics study

Mengdi Zhao [a], Jaeyoung Kim [b], Chunxian Guo [a,*], Joonkyung Jang [b,*]

[a] Department of Materials Science and Engineering, Suzhou University of Science and Technology, Suzhou 215009, PR China
[b] Department of Nanoenergy Engineering, Pusan National University, Busan 46241, Republic of Korea

ARTICLE INFO

Keywords:
Mussel adhesive proteins
L-3,4-dihydroxyphenylalanine
Graphite
Water resistant adhesion
Molecular dynamics simulation

ABSTRACT

Mussel adhesive proteins (MAPs) are prototypical water-resistant adhesives that can adhere to virtually any surfaces. Using all-atom molecular dynamics (MD) simulations, we study the molecular mechanisms behind the adhesions of two key MAPs: Mfp-5 from *Mytilus edulis* and Pvfp-5β from *Perna viridis*. We uncover the conformational dynamics and energetics underlying the adhesions of these proteins onto a hydrophobic graphite surface. Both MAPs adhere by contacting their l-3,4-dihydroxyphenylalanine (DOPA) residues with the surface. Mfp-5 adheres stronger than Pvfp-5β because of its flexibility in adjusting conformation to maximize the contact with the surface. Pvfp-5β protects the DOPA residues from oxidation by utilizing cysteine residues.

1. Introduction

Mussel adhesive proteins (MAPs) are prototypes of water-resistant adhesives because of their remarkable abilities to adhere to virtually any surfaces in water [1]. Among these, *Mytilus foot proteins* (Mfps) and *Perna viridis foot proteins* (Pvfps) in particular have strong adhesive properties in challenging marine environments [2–6]. Despite their distinctly different structural and functional characteristics, both Mfp and Pvfp proteins form durable and resilient underwater adhesions, which inspired extensive efforts to develop adhesives mimicking Mfp and Pvfp [7–8].

Understanding the molecular mechanism behind the adhesion of MAP will fundamentally impact the design and engineering of a water-resistant adhesive [9–11]. MAPs demonstrate remarkable adhesion even to hydrophobic surfaces such as graphite or Teflon [12]. This strong adhesion is primarily mediated by π–π interactions, as highlighted in the work of Qin et al. [13]. Additionally, Gebbie et al. demonstrated that cation–π interactions can play a significant role in enhancing adhesion in hydrophobic environments, complementing van der Waals interactions [14]. In our calculations, we employed graphite as the interface model due to its well-characterized electronic and structural properties, which make it an ideal substrate for studying π–π and related interactions. The π-electron system in graphite leads to quadrupole polarization effects and electron delocalization, which can influence interfacial interactions [15–16]. The quadrupole polarization of graphite can induce unique interfacial phenomena, including enhanced π–π interactions and potential charge transfer effects, which may influence the adhesion mechanisms of DOPA residues in MAPs.

In addition to π-π interactions, our study also highlights the role of σ-π interactions in the adhesion of MAPs. σ-π interactions occur when a σ-bond (e.g., a C—H bond) from one molecule interacts with the delocalized π-electron cloud of an aromatic ring [17]. These interactions stabilize adhesion, particularly when the phenyl rings of DOPA are tilted relative to the graphite surface due to molecular conformation changes, the hydration layer, or interference from other amino acid residues.

Another key factor influencing adhesion is the system's pH, which governs the ionization states of protein residues and the redox behavior of catechols. Variations in pH could dynamically affect the protonation states and redox activities of DOPA residues, potentially altering the underlying adhesion mechanisms [18]. Similarly, cation–π interactions are an important mode of interaction in MAPs. As highlighted in Dougherty et al. [19], these interactions can be up to three times stronger than typical salt bridges, such as those between charged lysine (Lys) and glutamate (Glu) residues. Lysine residues in close proximity to DOPA could engage in cation–π interactions with the π-electron system of graphite, further stabilizing the protein adhesion.

Another critical post-translational modification that may influence adhesion is the phosphorylation of serine (Ser) residues. Phosphorylation, a well-known regulatory mechanism, has been shown to modulate both adhesion strength and conformational flexibility in MAPs [20].

* Corresponding authors.
E-mail addresses: cxguo@usts.edu.cn (C. Guo), jkjang@pusan.ac.kr (J. Jang).

https://doi.org/10.1016/j.surfin.2025.105847
Received 13 October 2024; Received in revised form 16 December 2024; Accepted 15 January 2025
Available online 15 January 2025

Phosphorylation could alter the electrostatic environment and enhance or diminish interactions such as cation–π or π–π stacking. These aspects warrant further investigation, particularly through hybrid quantum–classical simulations to incorporate the effects of post-translational modifications [21]. Temperature, another environmental factor, plays a critical role in regulating adhesion by influencing protein flexibility, hydration layer dynamics, and conformational transitions [22]. Controlling temperature at 300 K in our simulations reflects physiological conditions and ensures that the adsorption behavior of MAPs can be studied under biologically relevant scenarios.

Despite the extensive studies on Mfps, Pvfps remain relatively underexplored. As the first protein secreted in the byssus formation of Perna viridis, Pvfp-5β plays a crucial role in the wet adhesion of Pvfp. Pvfp-5β is highly disordered in structure, having up to 43 % random coils. Pvfp-5β predominantly adopts a β-sheet extended structure, in sharp contrast with the α-helix-rich and globular structure of Mfp-5 [23]. The difference in structure presumably results in distinct adhesion mechanisms of these proteins [24]. Given its rapid and strong adhesion, Pvfp-5β serves as an ideal model for investigating the molecular mechanism for the adhesion of Pvfp.

Herein, we comparatively study the underwater adhesions of Mfp-5 and Pvfp-5β onto a graphite surface by using all-atom *molecular dynamics* (MD) simulation. Using the *replica exchange* MD (REMD) simulation combined with the umbrella sampling, we uncover the conformational dynamics and energetics underlying the adhesions of these proteins. We elucidate how the distinct structural features of Mfp-5 and Pvfp-5β influence their adhesion mechanisms and strengths. The present study not only builds upon the existing knowledge of Mfps but also shed new insights into the adhesion of Pvfp-5β, a less explored but equally important MAP. Understanding these fundamentals is crucial for development of the next-generation bio-inspired adhesives tailored for specific applications in wet environments [25]. Our findings are expected to provide a deeper understanding of the relationship between the protein structure and adhesion.

2. MD simulation details

2.1. General MD methods

All MD simulations were conducted by using Gromacs 5.1.4 software [26] under the NVT ensemble. The AMBER force field [27] was employed to model the Mfp-5, Mfp-3 or Pvfp-5β protein in the presence of an explicit water solvent described by the TIP3P model. A Mfp-5, Mfp-3 or Pvfp-5β protein was placed in a cubic simulation box with dimensions of 9.80 × 9.35 × 10.00 nm^3, solvated with 10,789 water molecules. This choice ensured full solvation of the protein and maintained a realistic water density of approximately 1 g/cm^3, which aligns with experimental observations and common practices in molecular dynamics simulations [28]. The TIP3P water model was selected for its compatibility with the AMBER force field and its ability to accurately represent the solvation environment.

The MD integration time step was set to 1.0 fs. We accounted for the long-ranged electrostatic interactions by using the particle-mesh Ewald (PME) method with a cutoff distance of 1.2 nm [29]. The short-ranged van der Waals (VDW) interactions were truncated at 1.2 nm as well, following standard practices in simulations employing the AMBER force field, which ensures the inclusion of all significant VDW interactions while maintaining computational efficiency [30]. While this approach effectively models van der Waals and electrostatic interactions, it does not explicitly parameterize cation–π interactions, which involve partially quantum mechanical effects and are not inherently captured by classical force fields like AMBER. This limitation suggests that some contributions from cation–π interactions may have been underestimated.

Additionally, the explicit water solvent in our simulation was modeled with a dielectric constant approximating that of bulk water (~80). This was chosen to represent a typical physiological aqueous environment and to ensure consistency with previous experimental and computational studies. However, mussel adhesive proteins are delivered through a liquid-liquid phase separation (LLPS) mechanism. This process creates a microenvironment with a dielectric constant potentially much lower than that of bulk water, which may significantly influence adhesion mechanisms. The LLPS-mediated low-dielectric environment can impact the ionization states of protein residues and the redox behavior of catechols, potentially altering the adhesion dynamics [31].

Despite this, the current model accurately captures the π–π stacking interaction and σ-π interaction between DOPA residues and the delocalized π-electron system of the graphite surface. The π-electron system, inherent to graphite's polyaromatic structure, not only facilitates π–π and σ-π interactions but also provides a suitable substrate for exploring cation–π interactions. As highlighted in Gebbie et al., cation–π interactions are particularly significant in systems involving adhesive proteins and can contribute to both cohesion and adhesion.

We maintained the system at 1 bar and 300 K by controlling temperature via coupling the system to a V-rescale thermostat with a relaxation time of 0.1 ps, ensuring efficient thermal equilibration. We applied the LINCS algorithm [32] to constrain all the bonds involving hydrogen atoms.

In simulating the adhesion, the graphite surface was modeled as a three-layer graphene sheet, with each layer spaced 3.4 Å apart, consistent with the interlayer distance in natural graphite. This configuration preserves the electronic and structural properties of bulk graphite while ensuring computational efficiency. The graphite surface was represented as uncharged and immobile sheets composed of sp^2-hybridized carbon atoms with a C—C bond length of 1.42 Å to reflect the experimental observations [33]. The interactions between the carbon atoms in graphite and the atoms in proteins were modeled using the *Lennard-Jones* (LJ) potential [34]. The periodic boundary conditions (PBCs) were applied in all three directions. To confirm the stability of the system under PBCs, we periodically monitored the density of water in the simulation box and checked for potential evaporation or adsorption effects. The results indicated no accumulation of water molecules on the underside of the graphene substrate, ensuring system stability throughout the simulation. We first performed the energy minimization by relaxing water molecules using the steepest descent method. This was followed by a 100-ps long NVT equilibration phase, during which the backbone atoms of the protein were restrained to allow the solvent molecules to equilibrate around the protein while minimizing structural changes to the protein itself. During this phase, the temperature stabilized at the target value of 300 K, confirming that the system was well-equilibrated and prepared for the subsequent production MD simulation. Finally, a 50-ns long production MD run was conducted without restraints. We visualized MD simulations by using PyMol [35] and Visual Molecular Dynamics (VMD) [36].

We calculated the *potential-of-mean force* (PMF) vs. the height (H) of the *center-of-mass* (COM) of protein measured from the graphite surface by using the umbrella sampling [37]. H was varied between 14 and 31 Å (200 windows) for Mfp-5 and between 11 and 44 Å (205 windows) for Pvfp-5β. We ran a 5 ns simulation for each window by applying a harmonic restraint with a force constant of 8000 kJ mol^{-1} nm^{-2}. The PMF profile was constructed using the weighted histogram analysis method [37].

2.2. Prediction of structure for Mfp-5

Using the known amino-acid sequence of Mfp-5 [38], we investigated the conformational dynamics of Mfp-5 by using the REMD method [39]. The present REMD simulation utilized 60 replicas with temperature ranging from 300 K to 507 K (with an interval of 3.5 K between successive replicas). This range and distribution of temperature were determined after preliminary testing to optimize the exchange efficiency between replicas. The Mfp-5 protein was placed in a cubic simulation

box solvated with 10,789 water molecules. The system was first equilibrated at 300 K and 1 bar for 200 ps under the NPT ensemble to achieve a proper density of water molecules. The equilibrated system served as the starting configuration for all replicas in the REMD simulation.

Following the initial equilibration, each replica was subjected to a short pre-simulation in the NVT ensemble to set the system to an assigned temperature. This ensured that each replica reached a thermal equilibrium at its designated temperature before the production phase of the REMD simulation [40]. Each replica was then simulated for 30 ns under the NVT condition. The replica exchanges were attempted every 2 ps, with an exchange frequency selected to balance between a computational efficiency and a thorough sampling. Each replica was simulated for 30 ns, but the final 20 ns portion was used for analysis, in order to minimize the influence of the initial condition.

The structure of Mfp-5 was generated by using the AMBER force field parameters. The tyrosine residues of Mfp-5 were post-translationally modified by adding hydroxyl groups to generate the DOPA residues, as described in the previous work [5]. The DOPA charge parameters were obtained from the AMBER general force field (GAFF). The bond, angle, dihedral, and LJ parameters were adopted directly from the AMBER force field [41]. We performed a conformational clustering using the g_cluster tool [42] of GROMACS with an RMSD cutoff of 0.9 nm. The most populated clusters were identified as representative structures and further analyzed for the adhesion mechanism of Mfp-5.

2.3. Prediction of structure for Pvfp-5β

The crystal structures of Pvfps, like those of Mfps, are currently unavailable [43–44]. However, Pvfp-5β shares a relatively high sequence similarity with the structural templates identified in the Protein Data Bank (PDB) database. Therefore, the structure of Pvfp-5β could be reliably modeled by using a standard protein homology modeling method. Herein, we used I-TASSER (Iterative Threading ASSEmbly Refinement) method [45] which integrates the template-based modeling with the *ab initio* techniques and generates a high-confidence structural model. The full-length amino acid sequence of Pvfp-5β was input into the I-TASSER server [46], an established platform for an automated prediction of a protein structure. This process started by selecting structural templates from the PDB database through threading with I-TASSER which utilizes diverse algorithms to increase the probability of identifying suitable templates for Pvfp-5β. The full structure of Pvfp-5β was assembled by aligning fragments derived from these templates. For regions where templates were unavailable, the *ab initio* modeling techniques were applied. The ab initio modeling involves an extensive conformational sampling by using the replica-exchange Monte Carlo simulation to identify the low-energy conformations.

The initial structures obtained above were refined by clustering similar conformations to select the most representative structures. By running MD simulations, we further improved the hydrogen-bonding network and resolved any steric clashes of the structural models. The overall quality of the models were enhanced by employing the FG-MD (Fragment-Guided Molecular Dynamics) method. We assessed the accuracy of the predicted structures by using a confidence score, called C-score, which evaluates the quality based on the significance of the template alignments and structural density. A C-score in the range of −1.5–2 gives a high global accuracy. The present model gave a C-score of 0.93.

3. Results and discussion

Fig. 1 illustrates four primary conformations of Mfp-5, each represented by different colors and annotated with the percentage of prevalence found in MD simulation. Conformer 1, which accounts for 40.2 % of all predicted structures, displays a disordered folding state characterized by a prominent α-helix and multiple irregular coils. This structure is similar to that reported by Qin et al. which consists of α-helices only [13]. Using RMSD-based clustering analysis with a cutoff threshold of 0.9 nm, we grouped conformations with high structural similarity and identified representative conformations with the lowest free energy for each cluster [13]. Conformer 1 emerged as the most prevalent and stable conformation, suggesting its significance during protein interaction with the graphite surface. Conformers 2 and 3 (comprising 14.7 % and 6.5 %, respectively) display β-sheets along with significant amounts of loops and coils. Conformer 4 make up 5.8 % and primarily consists of irregular coils and appears less frequently, indicating it is a secondary state. This clustering approach highlights the dynamic nature of Mfp-5, which adopts a disordered folded state, consistent with the absence of its crystal structure. We select the top-ranked Conformer 1 for further investigation on the structure and energetics in the underwater adhesion onto a graphite.

As illustrated in Fig. 2(a), Pvfp-5β has 6 β-sheets with coils. Unlike the globular structure of Mfp-5, it exhibits an extended and non-globular conformation. The DOPA residues are shown in orange. The DOPA residues are mainly located at the periphery of the protein, with their aromatic rings oriented toward the solvent. This orientation presumably facilitates the interaction of protein with the solvent molecules. The exposed aromatic rings, combined with the overall flexibility of the structure, provide numerous binding opportunities and thereby enhance the stability of protein in the adhesion.

Fig. 2(b) illustrates the surface of Pvfp-5β is predominantly covered with positive charge with a small portion of negative charge. The present structure of Pvfp-5β is similar to the one previously reported, reinforcing the validity of our structural prediction [24].

Fig 3 illustrates the dynamics of adhesion for both Mfp-5 and Pvfp-5β. Both the proteins, initially separated from the surface, firmly adhere to the surface within 50 ns. The initial structure is largely preserved in the final structure of protein adhered to the surface. For Mfp-5, three DOPA residues directly contact the surface by displacing water molecules pre-adsorbed. The initial interaction occurs at 20.9 ns, when the hydroxyl groups of the DOPA residues (Y17 and Y23) engage with the surface, starting the adsorption. By 36.4 ns, another DOPA residue (Y29) joins, further stabilizing the protein. Similarly, Pvfp-5β contacts the surface primarily through its DOPA residues. The DOPA labeled as Y2 firstly contacts the surface (0.2 ns). Later, two additional DOPAs (Y10

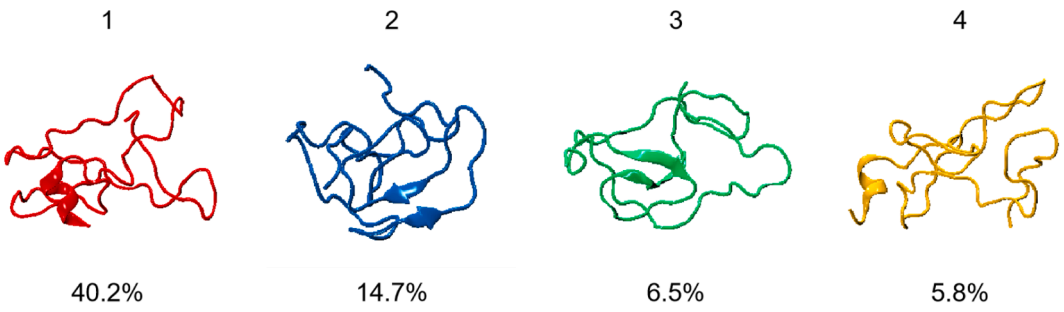

Fig. 1. Four primary conformations of Mfp-5 predicted from the current all-atom MD simulation. The Mfp-5 proteins are depicted in a Newcartoon style.

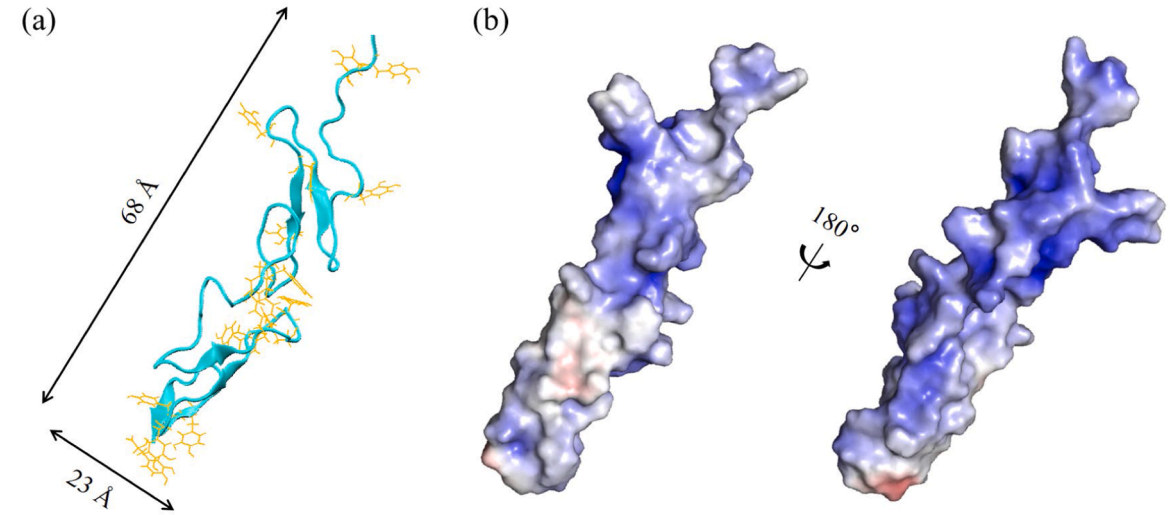

Fig. 2. (a) Conformation of Pvfp-5β predicted by the present homology modeling combined with MD simulation. The protein is depicted in a Newcartoon style. The DOPA residues are shown in orange. (b) Electrostatic potential maps of surface charge of Pvfp-5β. The surface potentials of anionic and cationic regions are illustrated in red and blue, respectively.

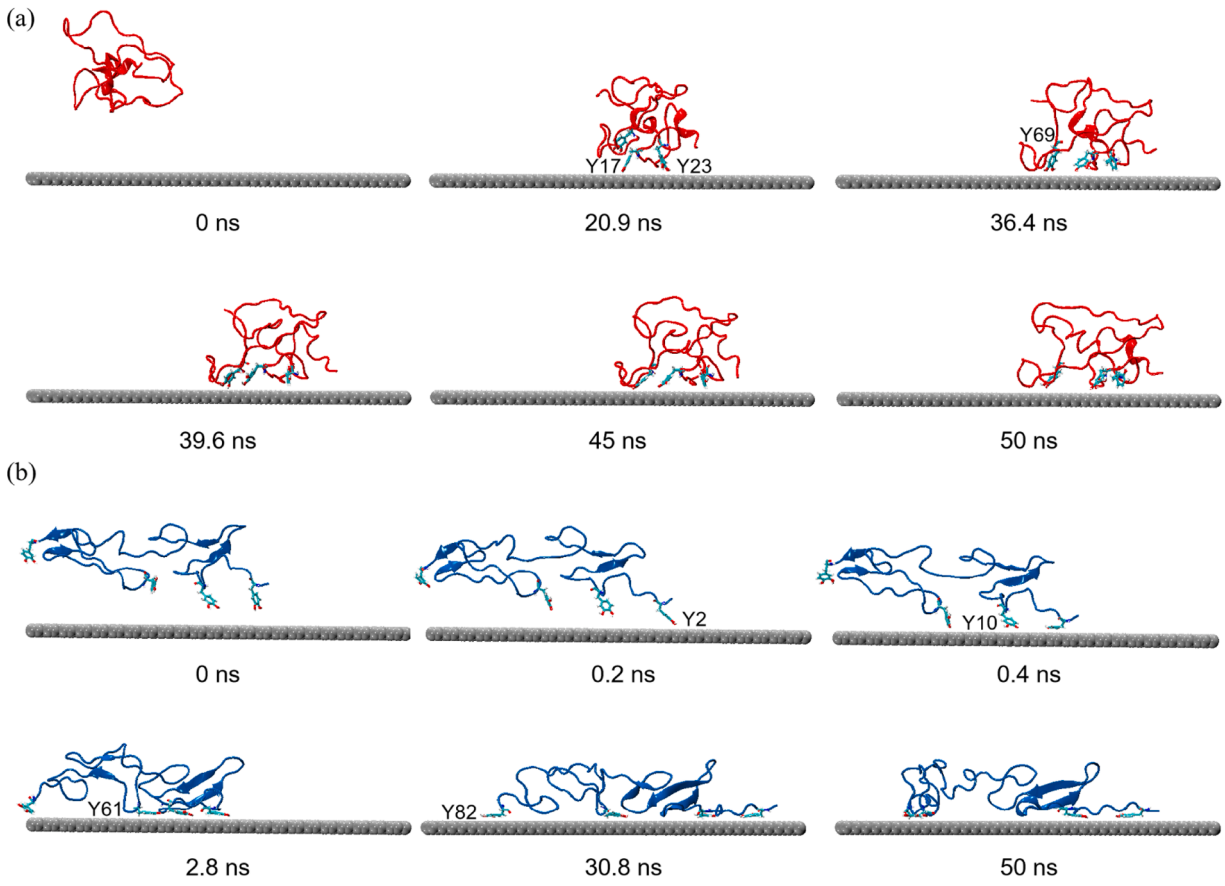

Fig. 3. Dynamics of the underwater adhesion of MAP to a graphite surface. Representative snapshots from MD simulations are displayed for the adhesions of Mfp-5 (a) and Pvfp-5β (b). The MAP proteins are depicted in a Newcartoon style, and the DOPA residues contacting the surface are shown in bond style. For visual clarity, water molecules and counter ions are omitted. Only the top layer of graphite is illustrated.

and Y81) sequentially adhere to the surface. Finally, another DOPA (Y82) adheres to the surface, resulting in four DOPAs in total involved in the adhesion.

Therefore, the DOPA residues are crucial in the adhesions of both Mfp-5 and Pvf-5β. The π-π interaction between the phenyl rings of DOPA and the graphite surface facilitates protein conformational adjustment, leading to stable adhesion. However, in Mfp-5, the phenyl rings of DOPA residues form an angle with the graphite surface rather than being perfectly parallel. This deviation is likely influenced by water molecules and neighboring amino acid residues, which can interfere with direct π-π interactions. Such interference alters molecular conformations, affects the structure of the hydration layer, or provides a shielding effect.

When the phenyl rings are tilted, σ/π interactions can occur. These involve a σ-bond (e.g., a C—H bond) interacting with the delocalized π-electron cloud of an aromatic ring, stabilizing adhesion even when the aromatic ring is not perfectly parallel to the surface. The strength of σ/π interactions depends on the distance and angle between the C—H bond and the aromatic plane, with optimal interactions occurring when the C—H bond is nearly perpendicular to the aromatic ring [17]. In our simulations, σ/π interactions compensate for the reduced π-π stacking efficiency in Mfp-5 when DOPA residues are tilted relative to the graphite surface.

Both π/π and σ/π interactions contribute to the overall adhesion of Mfp-5 and Pvfp-5β, albeit with differing efficiencies depending on molecular conformation. While π/π interactions dominate when DOPA residues are nearly parallel to the surface, σ/π interactions provide supplementary stabilization in tilted configurations [17].

In order to quantitatively examine the dynamics of adhesion, we track down the height of protein from the surface, H. As shown in Fig. 4 (a), the H of Mfp-5 noticeably fluctuates during the initial 20.9 ns. This fluctuation suggests that the Mfp-5 has not formed a stable adhesion to the surface, signifying a state of free diffusion or of weak interaction with the surface. At 20.9 ns, H suddenly drops because Mfp-5 initiates the contact with the surface. This initial anchoring is attributed to the contact of the hydroxyl groups of DOPA residues (Y17 and Y23) with the surface. As time progresses (36.4 ns), another DOPA residue (Y29) adheres, further stabilizing the adhesion of protein. By this time, the fluctuation of H diminishes, because all the three DOPA residues firmly adhered onto the surface. The protein undergoes conformational adjustments, characterized by partial unfolding to maximize the contact with the surface.

The time evolution of H for Pvfp-5β is shown in Fig. 4(b). Within the first few ns, H rapidly decreases to approximately 12 Å, indicating that Pvfp-5β quickly contacts the surface. This rapid decrease in H contrasts with that for Mfp-5. As all the DOPA residues adhere onto the surface, H gradually stabilizes after ~10 ns, signaling a stable state of adhesion. In this stabilization stage, the protein structurally adjusts to maximize its contact with the surface. In short, both Mfp-5 and Pvfp-5β establish multiple contacts with the surface via their DOPA residues.

We study the energetics of adhesion by constructing the PMF vs. H (Figs. 5 and 6). In the case of Mftp-5, the PMF shows a minimum around $H = 1.5$ nm, which corresponds to a firm adhesion. The subsequent rise in PMF with increasing H indicates an extra free energy needed to detach Mftp-5 from the surface. The PMF levels off around $H \geq 2.65$ nm, owing to a complete detachment of the protein from the surface. Therefore, the range of attraction in the PMF curve is 1.15 nm. The adhesion energy of Mfp-5, determined by the depth of the minimum in the PMF curve, is 28 kcal/mol. Also shown in Fig. 5 are the snapshots of 4 representative points in the PMF curve (drawn as symbols).

A reasonable measure of the strength of adhesion is the *adhesion energy per unit area* calculated as follows. We determine the *contact area* (CA) between the protein and surface [13] by using

$CA = (SAS_{protein} + SAS_{surface} - SAS_{complex})/2$ where $SAS_{protein}$, $SAS_{surface}$, and $SAS_{complex}$ are the solvent-accessible surface areas of the isolated protein, surface, and the protein-surface complex, respectively. The CA of Mfp-5 is 8 nm^2, and, therefore, the adhesion energy per unit area is 24.3 mJ/m^2, which is higher than the experimental value reported for the adhesion of Mfp-5 on a hydrophilic mica surface (9.0–13.7 mJ/m^2) [3]. This result aligns with previous findings, such as those mentioned in Levine et al.'s study [5], where it was observed that mussel foot proteins (Mfps) exhibit stronger adhesion on hydrophobic surfaces compared to hydrophilic ones. Graphite, being a hydrophobic substrate, provides a favorable environment for π–π stacking interactions and σ/π interactions between the aromatic rings of DOPA residues and the delocalized π-electron system of the graphite surface. This interaction is not only stronger but also longer-ranged compared to the hydrogen-bonding interactions that dominate on hydrophilic surfaces like mica.

The PMF profile of Pvfp-5β is shown in Fig. 6. Pvfp-5β firmly adheres at $H = 1.15$ nm, which is shorter than found for Mfp-5 (=1.5 nm). As H rises to 4.3 nm, the PMF increases and finally plateaus. The range of attraction to the surface is 3.15 nm, significantly larger than that of Mfp-5. The adhesion energy is found to be 48 kcal/mol. Note, in contrast to Mfp-5, the secondary structure of Pvfp-5β is disrupted in the process of detachment. Presumably, the enhanced adhesion energy of Pvfp-5β enforces a disruption of the secondary structure (maintained by hydrogen bonds) in the detachment from the surface. As the CA of Pvfp-5β is 16 nm^2, the adhesion energy per unit area is 20.8 mJ/m^2 for Pvfp-5β. Note, the adhesion energy of Pvfp-5β is greater than that of Mfp-5, but the adhesion energy area per unit area is smaller however. The present value is even larger than the experimental adhesion energies for Pvfp-5β on mica surfaces, 3.0–5.5 mJ/m^2 [24]. Therefore, Pvfp-5β, like Mfp-5, adheres to a hydrophobic surface as strongly to a hydrophilic surface. These proteins versatilely adhere onto both hydrophilic and hydrophobic surfaces. In our previous work, the DOPA residues adhere through multiple hydron bonds to a hydrophilic surface [47–49] In the case of a hydrophobic surface, the DOPA residues adheres via the π-π and σ/π interactions between their aromatic rings and the underlying surface [50].

Why Mfp-5 adheres more strongly than Pvfp-5β? A MAP protein's ability to establish compact contact with a surface is critical for stronger adhesion per unit area. Proteins with a lower molecular weight is expected to be more flexible, enabling them to maximize surface contact.. Given the molecular weight of Mfp-3 (6 kDa) is smaller than that of Mfp-5 (9 kDa) and Pvfp-5β (9.45 kDa). This higher flexibility allows Mfp-3 to achieve greater surface contact, resulting in the highest adsorption

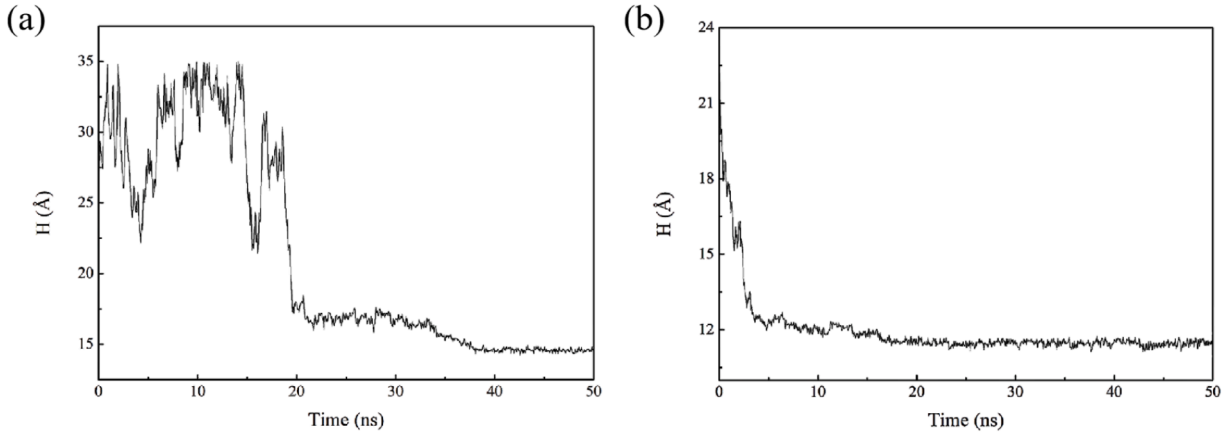

Fig. 4. Time evolution of the height of the COM of protein from the surface, H, for Mfp-5 (a) and Pvfp-5β (b).

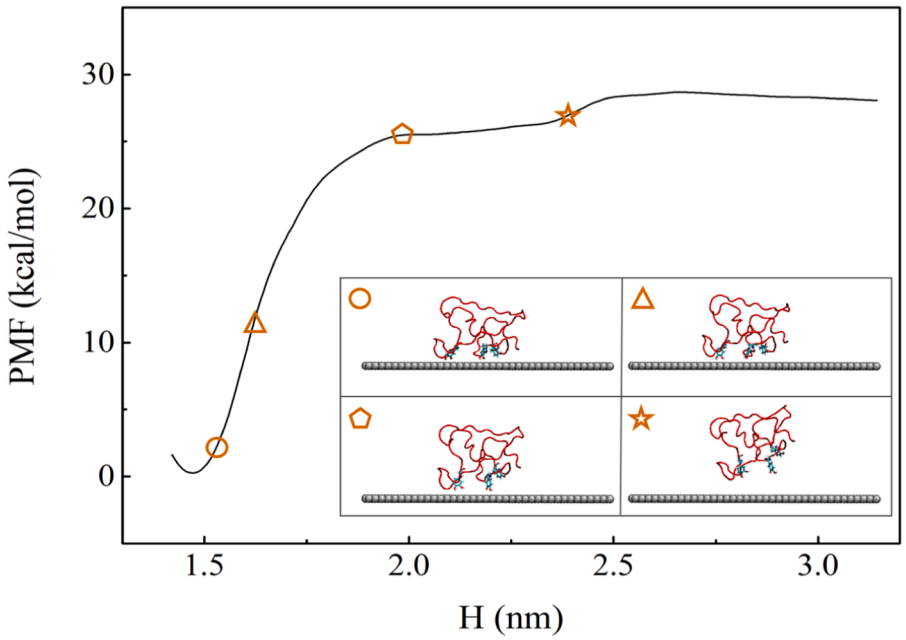

Fig. 5. Free energy profile for the underwater adhesion of Mfp-5 onto a graphite surface. Drawn is the PMF vs. the height of the COM of Mfp-5 from the surface, H. Representative snapshots are provided for four representative Hs (marked as symbols in the PMF curve).

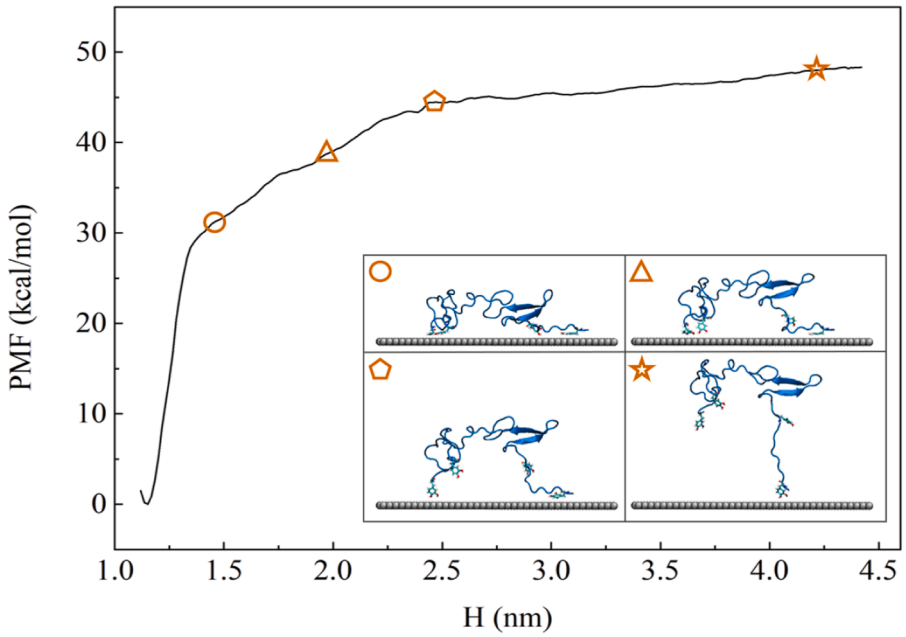

Fig. 6. The free energy profile for the underwater adhesion of Pvfp-5β onto a graphite surface. The PMF is plotted vs. the height of the COM of Pvfp-5β from the surface, H. Representative snapshots are provided for four distinct heights (marked as symbols) on the PMF curve.

energy per unit area among the three proteins. Conversely, Pvfp-5β, with its higher molecular weight and lower flexibility, has the weakest adhesion per unit area.

Beyond flexibility and molecular weight, other factors also contribute significantly to adhesion strength. The net charges of Mfp-5 and Pvfp-5β differ due to their amino acid compositions. Positively charged residues in Mfp-5, such as lysine and arginine, can enhance adhesion through electrostatic interactions with negatively charged or polar regions on the surface. In contrast, Pvfp-5β has fewer such residues, potentially weakening its adhesive capacity [24].

Hydrophobic interactions also play an important role. Mfp-5 contains hydrophobic residues such as phenylalanine and leucine, which contribute significantly to van der Waals interactions with the graphite surface, reinforcing adhesion. Pvfp-5β, however, has a lower proportion of hydrophobic residues, resulting in weaker hydrophobic interactions and reduced overall adhesion strength.

The combination of molecular mass and flexibility further influences adsorption strength. The lower molecular mass and greater flexibility of Mfp-5 allow it to rapidly adjust its conformation during adsorption, maximizing surface contact and adapting effectively to microscopic surface irregularities. In contrast, the larger molecular mass and reduced flexibility of Pvfp-5β limit its ability to achieve such conformational adjustments, resulting in fewer DOPA residues making direct contact with the surface.

Experimentally, Pvfp-5β is known to have the strongest adhesion among various Pvfps. According to the present calculation, Mfps should adhere stronger than Pvfps. It should be noted however that the present study focuses on the anchoring of a Pvfp or Mfp protein onto a surface. However, also important is the *curing* process where multiple proteins crosslink with each other to form a firm matrix at a much longer timescale (>hrs). Our results merely indicate that Mfps adhere more strongly at this initial anchoring stage of adhesion.

The adhesion energy of Mfp-5 observed in the present study is lower than the energy of Mfp-3 on hydrophobic surfaces previously reported by Qin et al. (28 mJ/m^2) [13]. In order to explain this difference, we examine the structures of Mfp-3 and Mfp-5 adhered to graphite (Fig. 7). Both Mfp-3 and Mfp-5 adhere by contacting three DOPA residues with the surface. Based on the work of Qin et al. [13], π–π stacking interactions are most effective when the aromatic rings are parallel to the graphite surface, as this orientation maximizes π-electron cloud overlap. In Mfp-3, this nearly parallel configuration (with angles <10°) significantly enhances π–π stacking interactions. However, the more upright orientation observed in Mfp-5 reduces π–π overlap and potentially weakens stacking interactions. The angles between the phenylene ring and graphite planes >45°, the interactions between the DOPA residues and the graphite surface likely involve a hybrid mechanism, combining contributions from both π–π stacking and σ/π interactions.

When the phenyl rings deviate from the parallel configuration, the interaction shifts from being predominantly π–π to including σ/π interactions. In this configuration, C–H bonds, such as those in the hydroxyl groups of DOPA, can interact with the delocalized π-electron cloud of the graphite surface. This type of interaction is supported by studies, including those by Alonso et al. [17], which highlight the importance of σ/π interactions in systems where aromatic rings are tilted relative to a surface. A similar finding was also reported in the previous quantum mechanical simulation of the wet adhesion of catechol onto a graphite [50].

Additionally, the hydration layer on the graphite surface may also contribute to the observed interaction. At intermediate orientations, the hydroxyl groups of DOPA could interact with water molecules within the hydration layer [51]. As the DOPA residues flatten to increase contact with the surface, dehydration of the surface may occur, enhancing the π–π and σ/π contributions. However, at an angle greater than 45°, this water-mediated interaction may play a more significant role alongside direct π–π and σ/π interactions. The greater tilt angle reduces π–π overlap, resulting in the adhesion energy of Mfp-5 being lower than that of Mfp-3.

We investigate how Mfp-5 and Pvfp-5β disrupt the *hydration layer* (HL) formed on graphite in the course of adhesion. On the graphite, a hydration layer naturally forms with a thickness of 7 Å, as confirmed by previous studies on water ordering near hydrophobic surfaces. By leveraging advanced computational techniques, specifically density grid mapping with Python, we provide a clearer visualization of water molecule distributions at the protein-graphite interface. This approach enables a more precise quantification of hydration dynamics and surface dehydration, which are essential factors in adhesion mechanisms. Shown in Fig. 8 are the water densities of HLs. In the progress of adhesion, the dehydrated region of HL expands over time for both Mfp-5 and Pvfp-5β. This dehydration process is critical, as the displacement of structured water molecules facilitates closer protein-surface contact and optimizes π–π interactions between the phenolic rings of DOPA residues and the graphite surface. Notice Pvfp-5β more pronouncedly dehydrates the HL. The dehydrated area finally stabilizes to 8 nm^2 and 16 nm^2 for Mfp-5 and Pvfp-5β, respectively. Notably, the dehydrated areas exactly match those calculated by using the solvent-accessible areas (see above), meaning each protein displaces water molecules pre-adsorbed to contact with the surface.

As DOPA residues approach the graphite surface, their hydroxyl groups initially interact with the structured hydration layer, contributing indirectly to adhesion by promoting localized dehydration. This dynamic interaction aligns with observations that hydration layer dynamics play a critical role in the initial stages of protein adhesion. Our model predicts a transition during this process: as water molecules are displaced, π–π stacking interactions between the phenolic rings of DOPA and the graphite surface become dominant. This transition is accompanied by localized disruption of the hydration layer, further enhancing direct protein-surface contact.

Additionally, when the phenolic rings of DOPA are tilted relative to the graphite surface, σ–π interactions between C—H bonds and the delocalized π-electron cloud of graphite play a supplementary role. These interactions compensate for the reduced efficiency of π–π stacking under such configurations, as demonstrated in our simulations. The interplay between hydration layer dynamics, localized surface dehydration, and the transition from hydration-mediated to π–π and σ–π interactions underpins the molecular mechanisms driving adhesion in both Mfp-5 and Pvfp-5β.

Pvfp-5β contain a significant amount of cysteine (15–20 mol%), and experimental findings suggest that cysteine (Cys) presumably prevent the oxidation of DOPA. We observe, as DOPA10 approaches the surface, Cys12 aids in displacing the preexisting water molecules and in creating a dehydrated area that allows the DOPA residue to contact the surface (Fig. 9(a)). Once both the DOPA and Cys residues adhere onto the surface (Fig. 9(b)), the surrounding water molecules are effectively displaced. Therefore, the Cys residue facilitates the adhesion of Pvfp-5β. Our finding is in accord with the prior experiments [52–53] which reported that Pvfp-5 protects its DOPA residues from oxidation by forming the cysteine-DOPA bonds and disulfide bridges within the adhesive plaque [54].

Yu et al. demonstrated that Cys thiols in Mfp-6 significantly enhance the adhesion of Mfp-3 to mica surfaces by sacrificially reducing oxidized DOPAquinone back to its adhesive form [55]. In Mytilus, this protection is provided by a separate molecule (Mfp-6), whereas in Pvfp-5β, the Cys residues coexist with DOPA on the same protein backbone, potentially streamlining the adhesive and protective functions. This co-location of

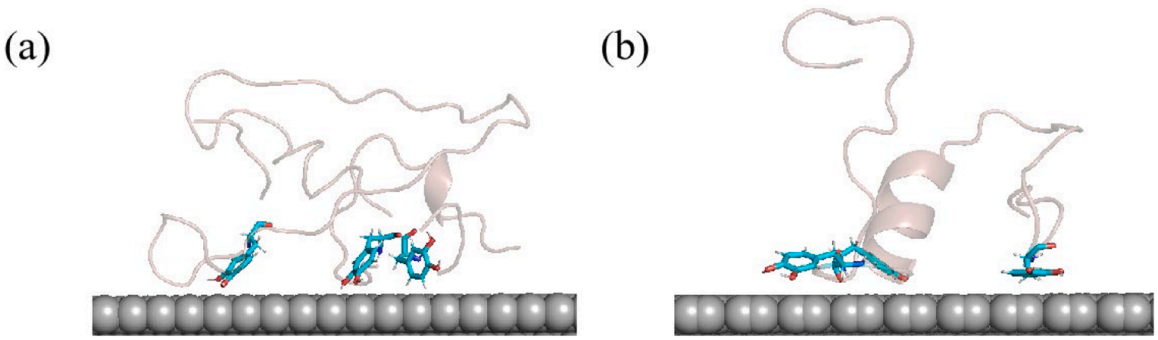

Fig. 7. MD snapshots of Mfp-5 (a) and Mfp-3 (b) adhered to a graphite surface. The DOPA residues adsorbed on the surface are displayed in bond style.

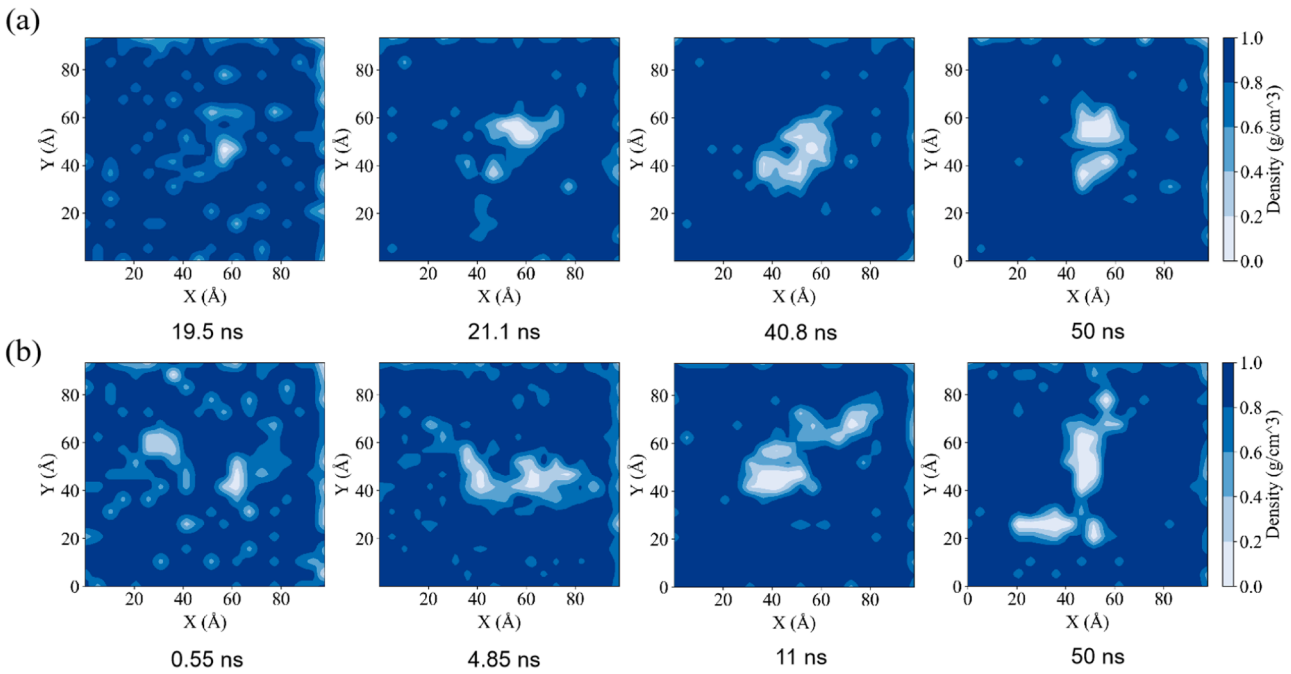

Fig. 8. Time progressions of the hydration layers in the adhesions of Mfp-5 (a) and Pvfp-5β (b). Shown in each panel is the distribution of the density of water molecules within 7 Å from the surface. The density of water is color mapped (blue and white indicate high and zero densities, respectively).

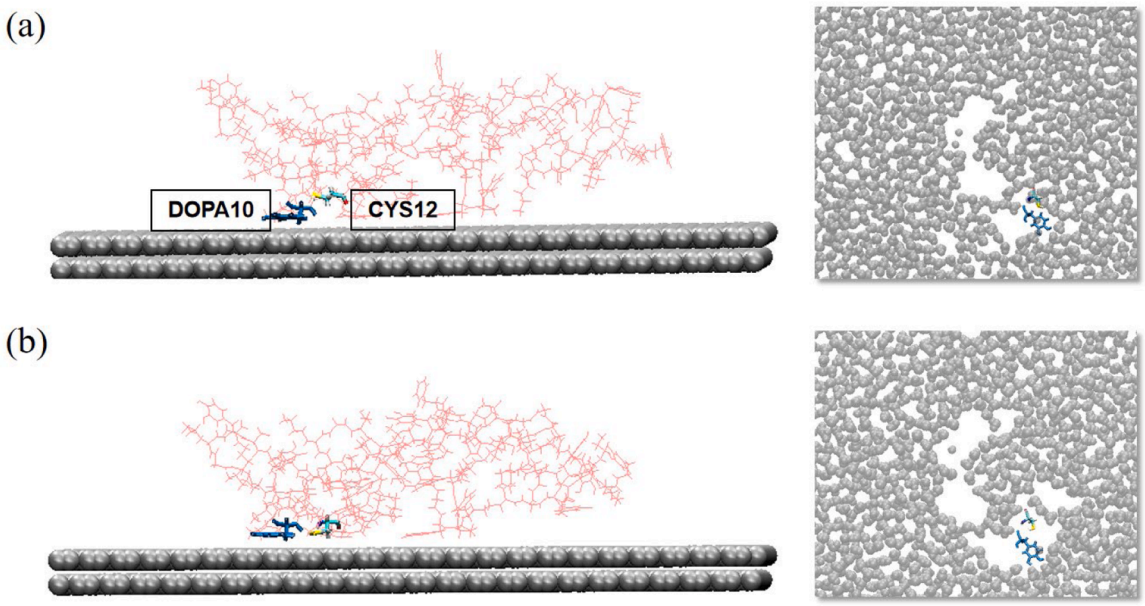

Fig. 9. (a) MD snapshot of Pvfp-5β adhering to a graphite. Shown in bond style is a DOPA residue (DOPA10) aided by cysteine (CYS12) nearby. (b) Snapshot of Pvfp-5β completely adhered to the surface. The structure of protein is represented in line style. In the right, water molecules within a height < 7 Å from the surface are shown in gray.

functional groups may enhance the efficiency of Pvfp-5β under oxidative conditions.

Additionally, the hydrophobic nature of cysteine thiols, as highlighted by Tanford & Nozaki, supports their contribution to surface dehydration, which is crucial for promoting DOPA's adhesion through π-π stacking interactions [56]. The thiols' propensity for oxidation at pH > 6 suggests that they act optimally under slightly acidic or neutral pH conditions, a hypothesis corroborated by the pH-dependent adhesion behavior observed in related systems.

4. Conclusion

With the help of all-atom MD simulation, we performed a comparative study on the mechanism and dynamics behind the underwater adhesion of Mfp-5 and Pvfp-5β onto a graphite surface. We presented the molecular insights into the structural and energetic aspects of the adhesion, giving a deeper understanding of the mechanism of adhesion. Our findings highlight the critical roles of DOPA residues, hydration dynamics, and protein conformational flexibility in driving effective adhesion to hydrophobic surfaces.

Mfp-5 adheres more strongly than Pvfp-5β. Because Mfp-5 is more

flexible, the DOPA residues of Mfp-5 adjust their orientations. The cysteine residues of Pvfp-5β facilitate displacing water molecules pre-adsorbed on the surface to create favorable conformation of the DOPA for adhesion. The present study unveils the molecular mechanisms underlying the underwater adhesion of MAP on a hydrophobic surface. These insights presumably impact the design of biomimetic materials with enhanced adhesive properties, potentially leading to the development of new adhesives for underwater applications. By elucidating the complementary roles of π–π, σ–π, and cation–π interactions, along with hydration layer dynamics, provide a foundation for engineering adhesives optimized for diverse applications, such as biomedical adhesives, underwater construction, and soft robotics. Furthermore, the demonstrated effectiveness of multi-residue interactions opens new pathways for designing hybrid adhesive formulations that combine strength, durability, and resistance to environmental challenges. The future work will focus on exploring the synergetic effects of residues other than DOPA and their contribution to the wet adhesion.

CRediT authorship contribution statement

Mengdi Zhao: Writing – original draft, Visualization, Validation, Software, Methodology, Funding acquisition, Data curation, Conceptualization. **Jaeyoung Kim:** Visualization, Validation, Software, Investigation, Data curation. **Chunxian Guo:** Writing – review & editing, Supervision, Investigation. **Joonkyung Jang:** Writing – review & editing, Supervision, Resources, Methodology, Funding acquisition, Formal analysis, Conceptualization.

Declaration of competing interest

The authors declare the following financial interests/personal relationships which may be considered as potential competing interests: Joonkyung Jang reports financial support was provided by National Research Foundation of Korea. Joonkyung Jang reports financial support was provided by Korea Evaluation Institute of Industrial Technology. Mengdi Zhao reports financial support was provided by National Science Foundation of Jiangsu Providence for Youths. Chunxian Guo reports financial support was provided by National Natural Science Foundation of China. If there are other authors, they declare that they have no known competing financial interests or personal relationships that could have appeared to influence the work reported in this paper.

Acknowledgments

This research was supported by Natural Science Foundation of Jiangsu Province for Youths (BK20230662). This work was also supported by the National Research Foundation of Korea (NRF) grant funded by the Korea government (MSIT) (no. 2021R1A2C1010936) and by the Korea Planning & Evaluation Institute of Industrial Technology and funded by the Korean government (Ministry of Trade, Industry, and Energy, Ministry of Science and ICT, Ministry of the Interior and Safety, National Fire Agency, Project Title: Development of gas hydrate extinguishing agent and fire suppression technology for inaccessible fires, Project Number: 2760000002). This work was also supported by National Natural Science Foundation of China (22372113).

Data availability

Data will be made available on request.

References

[1] D. Wu, X. Sun, X. Liu, L. Liu, R. Zhang, Simple-effective strategy for surface modification via annealing treatment polydopamine coating, Appl. Surf. Sci. 567 (2021) 150813.
[2] Q. Lin, D. Gourdon, C. Sun, N. Holten-Andersen, T.H. Anderson, J.H. Waite, J. N. Israelachvili, Adhesion mechanisms of the mussel foot proteins mfp-1 and mfp-3, Proc. Natl. Acad. Sci. 104 (2007) 3782–3786.
[3] J. Yu, Y. Kan, M. Rapp, E. Danner, W. Wei, S. Das, D.R. Miller, Y. Chen, J.H. Waite, J.N. Israelachvili, Adaptive hydrophobic and hydrophilic interactions of mussel foot proteins with organic thin films, Proc. Natl. Acad. Sci. 110 (2013) 15680–15685.
[4] S. Seo, S. Das, P.J. Zalicki, R. Mirshafian, C.D. Eisenbach, J.N. Israelachvili, J. H. Waite, B.K. Ahn, Microphase behavior and enhanced wet-cohesion of synthetic copolyampholytes inspired by a mussel foot protein, J. Am. Chem. Soc. 137 (2015) 9214–9217.
[5] Z.A. Levine, M.V. Rapp, W. Wei, R.G. Mullen, C. Wu, G.H. Zerze, J. Mittal, J. H. Waite, J.N. Israelachvili, J.-E. Shea, Surface force measurements and simulations of mussel-derived peptide adhesives on wet organic surfaces, Proc. Natl. Acad. Sci. 113 (2016) 4332–4337.
[6] K. Deepankumar, Q. Guo, H. Mohanram, J. Lim, Y. Mu, K. Pervushin, J. Yu, A. Miserez, Liquid–liquid phase separation of the green mussel adhesive protein Pvfp-5 is regulated by the post-translated dopa amino acid, Adv. Mater. 34 (2022) 2103828.
[7] C. Cui, T. Wu, X. Chen, Y. Liu, Y. Li, Z. Xu, C. Fan, W. Liu, A janus hydrogel wet adhesive for internal tissue repair and anti-postoperative adhesion, Adv. Funct. Mater 30 (2020) 2005689.
[8] M.Lo Presti, G. Rizzo, G.M. Farinola, F.G. Omenetto, Bioinspired biomaterial composite for all-water-based high-performance adhesives, Adv. Sci. 8 (2021) 2004786.
[9] T. Wang, J. Bai, M. Lu, C. Huang, D. Geng, G. Chen, L. Wang, J. Qi, W. Cui, L. Deng, Engineering immunomodulatory and osteoinductive implant surfaces via mussel adhesion-mediated ion coordination and molecular clicking, Nat. Commun. 13 (2022) 160.
[10] S. Xu, M. Kang, X. Xin, J. Liang, H. Xiao, Y. Lu, J. Yang, H. Zhai, Design principles and application research of mussel-inspired materials: a review, J. Environ. Chem. Eng. (2023) 111655.
[11] T. Priemel, G. Palia, F. Förste, F. Jehle, S. Sviben, I. Mantouvalou, P. Zaslansky, L. Bertinetti, M.J. Harrington, Microfluidic-like fabrication of metal ion–cured bioadhesives by mussels, Science 374 (2021) 206–211.
[12] W. Wei, J. Yu, C. Broomell, J.N. Israelachvili, J.H. Waite, Hydrophobic enhancement of dopa-mediated adhesion in a mussel foot protein, J. Am. Chem. Soc. 135 (2013) 377–383.
[13] Z. Qin, M.J. Buehler, Molecular mechanics of mussel adhesion proteins, J. Mech. Phys. Solid. 62 (2014) 19–30.
[14] M.A. Gebbie, W. Wei, A.M. Schrader, T.R. Cristiani, H.A. Dobbs, M. Idso, B. F. Chmelka, J.H. Waite, J.N. Israelachvili, Tuning underwater adhesion with cation–π interactions, Nat. Chem. 9 (2017) 473–479.
[15] X. Zhao, J.K. Johnson, An effective potential for adsorption of polar molecules on graphite, Mol. Simul. 31 (2005) 1–10.
[16] J. Luo, J. Lai, N. Zhang, Y. Liu, R. Liu, X. Liu, Tannic acid induced self-assembly of three-dimensional graphene with good adsorption and antibacterial properties, ACS Sustain. Chem. Eng. 4 (2016) 1404–1413.
[17] M. Alonso, T. Woller, F.J. Martín-Martínez, J. Contreras-García, P. Geerlings, F. De Proft, Understanding the fundamental role of π/π, σ/σ, and σ/π dispersion interactions in shaping carbon-based materials, Chem. Eur. J. 20 (2014) 4931–4941.
[18] O. Krivosheeva, A. Dėdinaitė, P.M. Claesson, Adsorption of Mefp-1: influence of pH on adsorption kinetics and adsorbed amount, J. Colloid Interface Sci. 379 (2012) 107–113.
[19] J.P. Gallivan, D.A. Dougherty, Cation-π interactions in structural biology, Proc. Natl. Acad. Sci. 96 (1999) 9459–9464.
[20] M.T. Bueno-Carrasco, J. Cuéllar, M.I. Flydal, C. Santiago, T.-A. Kråkenes, R. Kleppe, J.R. López-Blanco, M. Marcilla, K. Teigen, S. Alvira, Structural mechanism for tyrosine hydroxylase inhibition by dopamine and reactivation by Ser40 phosphorylation, Nat. Commun. 13 (2022) 74.
[21] J.H. Waite, X. Qin, Polyphosphoprotein from the adhesive pads of Mytilus edulis, Biochemistry 40 (2001) 2887–2893.
[22] R. Loayza-Muro, R. Elías-Letts, Responses of the mussel Anodontites trapesialis (Unionidae) to environmental stressors: effect of pH, temperature and metals on filtration rate, Environ. Pollut. 149 (2007) 209–215.
[23] X. Ou, B. Xue, Y. Lao, Y. Wutthinitikornkit, R. Tian, A. Zou, L. Yang, W. Wang, Y. Cao, J. Li, Structure and sequence features of mussel adhesive protein lead to its salt-tolerant adhesion ability, Sci. Adv. 6 (2020) eabb7620.
[24] L. Petrone, A. Kumar, C.N. Sutanto, N.J. Patil, S. Kannan, A. Palaniappan, S. Amini, B. Zappone, C. Verma, A. Miserez, Mussel adhesion is dictated by time-regulated secretion and molecular conformation of mussel adhesive proteins, Nat. Commun. 6 (2015) 8737.
[25] K. Li, Z. Xu, X. Liu, Y. He, X. Tian, X. Xu, G. Bo, S. Yuan, L. Xu, M. Yang, Mussel foot inspired bionic adhesive material enhanced by a reconstructed in vitro system for interfacial adhesion, Chem. Eng. J. 452 (2023) 139580.
[26] M.J. Abraham, T. Murtola, R. Schulz, S. Páll, J.C. Smith, B. Hess, E. Lindahl, GROMACS: high performance molecular simulations through multi-level parallelism from laptops to supercomputers, SoftwareX 1 (2015) 19–25.
[27] J.A. Maier, C. Martinez, K. Kasavajhala, L. Wickstrom, K.E. Hauser, C. Simmerling, ff14SB: improving the accuracy of protein side chain and backbone parameters from ff99SB, J. Chem. Theory Comput. 11 (2015) 3696–3713.
[28] E. Ritter, D. Yordanova, T. Gerlach, I. Smirnova, S. Jakobtorweihen, Molecular dynamics simulations of various micelles to predict micelle water partition equilibria with COSMOmic: influence of micelle size and structure, Fluid Phase Equilib 422 (2016) 43–55.

[29] T. Darden, D. York, L. Pedersen, Particle mesh Ewald: an N· log (N) method for Ewald sums in large systems, J. Chem. Phys. 98 (1993) 10089–10092.
[30] V. Sresht, A. Govind Rajan, E. Bordes, M.S. Strano, A.A.H. Padua, D. Blankschtein, Quantitative modeling of MoS2–solvent interfaces: predicting contact angles and exfoliation performance using molecular dynamics, J. Phys. Chem. C 121 (2017) 9022–9031.
[31] M. Ahmad, W. Gu, T. Geyer, V. Helms, Adhesive water networks facilitate binding of protein interfaces, Nat. Commun. 2 (2011) 261.
[32] B. Hess, H. Bekker, H.J.C. Berendsen, J.G.E.M. Fraaije, LINCS: a linear constraint solver for molecular simulations, J. Comput. Chem. 18 (1997) 1463–1472.
[33] J.-C. Charlier, X. Gonze, J.-P. Michenaud, Graphite interplanar bonding: electronic delocalization and van der Waals interaction, Europhys. Lett. 28 (1994) 403.
[34] S. Wang, S. Li, Z. Cao, T. Yan, Molecular dynamic simulations of ionic liquids at graphite surface, J. Phys. Chem. C 114 (2009) 990–995.
[35] W.L. DeLano, Pymol: an open-source molecular graphics tool, CCP4 Newsl. Protein Crystallogr. 40 (2002) 82–92.
[36] W. Humphrey, A. Dalke, K. Schulten, VMD: visual molecular dynamics, J. Mol. Graph. 14 (1996) 33–38.
[37] M. Souaille, B. Roux, Extension to the weighted histogram analysis method: combining umbrella sampling with free energy calculations, Comput. Phys. Commun. 135 (2001) 40–57.
[38] J.H. Waite, X. Qin, Polyphosphoprotein from the adhesive pads of Mytilus edulis, Biochemistry 40 (2001) 2887–2893.
[39] T. Terakawa, T. Kameda, S. Takada, On easy implementation of a variant of the replica exchange with solute tempering in GROMACS, J. Comput. Chem. 32 (2011) 1228–1234.
[40] Y.M. Rhee, V.S. Pande, Multiplexed-replica exchange molecular dynamics method for protein folding simulation, Biophys. J. 84 (2003) 775–786.
[41] G.A. Khoury, J.P. Thompson, J. Smadbeck, C.A. Kieslich, C.A. Floudas, Forcefield_PTM: ab initio charge and AMBER forcefield parameters for frequently occurring post-translational modifications, J. Chem. Theory Comput. 9 (2013) 5653–5674.
[42] X. Daura, K. Gademann, H. Schäfer, B. Jaun, D. Seebach, W.F. van Gunsteren, The β-peptide hairpin in solution: conformational study of a β-hexapeptide in methanol by NMR spectroscopy and MD simulation, J. Am. Chem. Soc. 123 (2001) 2393–2404.
[43] R.Y. Floriolli, J. von Langen, J.H. Waite, Marine surfaces and the expression of specific byssal adhesive protein variants in Mytilus, Mar. Biotechnol. 2 (2000) 352–363.
[44] H. Zhao, J. Sagert, D.S. Hwang, J.H. Waite, Glycosylated hydroxytryptophan in a mussel adhesive protein from Perna viridis, J. Biol. Chem. 284 (2009) 23344–23352.
[45] Y. Zhang, I-TASSER server for protein 3D structure prediction, BMC Bioinformat. 9 (2008) 1–8.
[46] J. Yang, Y. Zhang, I-TASSER server: new development for protein structure and function predictions, Nucl. Acid. Res. 43 (2015) W174–W181.
[47] S.A. Mian, L.C. Saha, J. Jang, L. Wang, X. Gao, S. Nagase, Density functional theory study of catechol adhesion on silica surfaces, J. Phys. Chem C. 114 (2010) 20793–20800.
[48] S.A. Mian, X. Gao, S. Nagase, J. Jang, Adsorption of catechol on a wet silica surface: density functional theory study, Theo. Chem. Acc. 130 (2011) 333–339.
[49] N. Ilyas, S.A. Mian, A. Rauf, E. Ahmed, G. Rahman, A. Sannyal, J. Jang, Stimulated reversal of the strong adhesion of catechol onto a silica surface, Bull. Korea. Chem. Soc. 43 (2022) 210–214.
[50] R.K. Chitumalla, K. Kim, X. Gao, J. Jang, A density functional theory study on the underwater adhesion of catechol onto a graphite surface, Phys. Chem. Chem. Phys. 23 (2021) 1031–1037.
[51] D. Ringe, G.A. Petsko, Mapping protein dynamics by X-ray diffraction, Prog. Biophys. Mol. Biol. 45 (1985) 197–235.
[52] Y. He, Y. Chang, J.C. Hower, J. Zheng, S. Chen, S. Jiang, Origin of repulsive force and structure/dynamics of interfacial water in OEG–protein interactions: a molecular simulation study, Phys. Chem. Chem. Phys. 10 (2008) 5539–5544.
[53] J. Zheng, L. Li, H.-K. Tsao, Y.-J. Sheng, S. Chen, S. Jiang, Strong repulsive forces between protein and oligo (ethylene glycol) self-assembled monolayers: a molecular simulation study, Biophys. J. 89 (2005) 158–166.
[54] M. Cui, S. Ren, S. Wei, C. Sun, C. Zhong, Natural and bio-inspired underwater adhesives: current progress and new perspectives, APL Mater 5 (2017) 116102.
[55] J. Yu, W. Wei, E. Danner, R.K. Ashley, J.N. Israelachvili, J.H. Waite, Mussel protein adhesion depends on interprotein thiol-mediated redox modulation, Nat. Chem. Biol. 7 (2011) 588–590.
[56] Y. Nozaki, C. Tanford, The solubility of amino acids, diglycine, and triglycine in aqueous guanidine hydrochloride solutions, J. Biol. Chem. 245 (1970) 1648–1652.